PNAS
www.pnas.org

Supplementary Information for

How Cholesterol Stiffens Unsaturated Lipid Membranes

Saptarshi Chakraborty, Milka Doktorova, Trivikram R. Molugu, Frederick A. Heberle, Haden L. Scott, Boris Dzikovski, Michihiro Nagao, Laura-Roxana Stingaciu, Robert F. Standaert, Francisco N. Barrera, John Katsaras, George Khelashvili, Michael F. Brown, and Rana Ashkar

* Rana Ashkar and * Michael F. Brown
Email: ashkar@vt.edu or mfbrown@u.arizona.edu

This PDF file includes:

Supplementary text
Figures S1 to S9
Tables S1 to S5
SI References

Materials and Sample Preparation

Synthesis of Perdeuterated Lipids. DOPC-d_{66} was synthesized from an *sn*-glycero-3-phosphocholine $CdCl_2$ complex (GPC•$CdCl_2$, Santa Cruz Biotechnology, Dallas, TX) and oleic acid-d_{34} (98% D, Sigma-Aldrich, St. Louis, MO) by the method of Mena & Djerassi (1) using dry toluene and dry ethanol-free chloroform (Sigma-Aldrich). In a representative procedure, GPC•$CdCl_2$ (490 mg, 1.11 mmol) was dried by rotary evaporation from toluene (3×5 mL), followed by storage *in vacuo* for 2 h, then suspended in 5 mL of chloroform (8 mL) with ultrasonication. Oleic acid-d_{34} (725 µL, 722 mg, 2.28 mmol, 2.05 equiv) was added via syringe, followed by a solution of *N*,*N*'-dicyclohexylcarbodiimide (1.41 g, 6.84 mmol, 6.15 equiv) in chloroform (2 mL) added in portions while swirling. *N*,*N*-dimethylaminopyridine (279 mg, 2.28 mmol, 2.05 equiv) was added as a solid and dissolved by swirling the solution, which was then sonicated for ≈ 18 h. After sonication, TLC was performed indicating substantial completion of the reaction. The TLC analysis was carried out on silica gel plates with 65:25:4 $CHCl_3$:MeOH:H_2O (v:v:v) as the mobile phase and iodine for visualization. The product was purified by chromatography on silica gel using sequential elution with 65:25:0, 65:25:2 and 65:25:3 (v:v:v) $CHCl_3$:MeOH:H_2O. Fractions containing DOPC-d_{66} (as judged by TLC) were pooled and rotary evaporated. To remove trace metal ions and acidic

www.pnas.org/cgi/doi/10.1073/pnas.2004807117

impurities, the residue was taken up in a mixture of 10 mL of chloroform, 20 mL of methanol, and 8 mL of aqueous buffer containing Tris (30 mmol/L or mM) and EDTA (20 mM) at pH 8.0. The mixture was shaken for 2 min in a separatory funnel, after which, additional chloroform (10 mL) and water (10 mL) were added to induce phase separation. The chloroform (lower) phase was washed 3× with 10 mM NaCl, dried over Na_2SO_4, and rotary evaporated to dryness. The combined yield from two preparations using 1.97 g of oleic acid-d_{34} was 1.20 g (45%) of DOPC-d_{66}.

Synthesis of Perdeuterated Cholesterol. The synthesis of perdeuterated cholesterol (Chol-d_{40}) was adapted from the protocol by H. Riezman (University of Geneva) and as described by Nickels et al. (2) The protocol uses genetically modified *Saccharomyces cerevisiae* RH682941 to produce cholesterol rather than ergosterol. This was established by culturing *S. cerevisiae* RH682941 in a medium containing yeast nitrogen base (7 g/L), yeast extract (5 g/L), D-glucose (12.5 g/L), uracil (30 mg/L), and L-leucine (30 mg/L) in D_2O. 1-L cultures were each inoculated with 0.5 mL of an overnight culture grown in a yeast extract peptone dextrose (YPD)–H_2O medium. The cultures were shaken at 30 °C for 4 days during growth, after which the cells were harvested by centrifugation (5,000 × g, 10 min) and washed once with water. The wet cell pellet (≈ 8 g) was resuspended in alcoholic potassium hydroxide (45.2 g of potassium hydroxide and 0.3 g of pyrogallol dissolved in 17 mL of water, then diluted with 100 mL of absolute ethanol) and refluxed for 2 h. An additional 25 mL of absolute ethanol was added, and the suspension was refluxed for an additional 1 h. After cooling to room temperature, the mixture was diluted with water (40 mL) and extracted with 3 × 35 mL of *n*-heptane. The combined heptane extracts were dried using a rotary evaporator, re-dissolved in a small amount of chloroform, and chromatographed on a column of silica gel packed with and eluted with 4:1 hexane: ethyl acetate. Fractions containing substantially pure cholesterol, as judged by TLC on silica gel (4:1 hexane: ethyl acetate eluent, phosphomolybdic acid stain), were combined and evaporated to dryness. The cholesterol was further purified by recrystallization twice from methanol. Gas chromatography/mass spectrometry (GC/MS) was performed after conversion of the cholesterol to its trimethylsilyl derivative using N,O-bis(trimethylsilyl)trifluoroacetamide containing 1% chlorotrimethylsilane (60 °C, 30 min). The CG/MS analysis showed 87% substitution of D for H, which corresponds, on average, to 40 deuterium atoms per cholesterol molecule.

Preparation of Large Unilamellar Vesicles (LUVs) for SAXS/SANS and NSE experiments. Aqueous lipid dispersions of LUVs were prepared by first mixing the required amounts of lipids and cholesterol in chloroform. All samples were prepared with a mole fraction of 4% (or 4 mol%) DOPS (1,2-dioleoyl-*sn*-glycero-3-phospho-L-serine) to avoid multilamellar stack formation (3) as shown in Fig. S1A. The solvent was evaporated with an inert gas stream and the sample placed under vacuum overnight. The dry lipid film was hydrated with a 10 mM sodium phosphate (NaP_i) pH 8.0 buffer (prepared with D_2O) at room temperature with intermittent vortex mixing. The suspension was then subjected to at least 5 freeze/thaw cycles using a – 80 °C freezer and a warm 40 °C water bath. Following that, the suspension was extruded through a polycarbonate filter (pore size of 100 nm or 50 nm) using an automated mini-extruder (Avanti Polar Lipids), by passing the suspension through the filter 31 times – yielding unilamellar vesicles, as confirmed by SAXS (Fig. S1A).

Preparation of Multilamellar Stacks for NMR Measurements. Solid state ^2H NMR samples were prepared using custom-built glass NMR tubes by mixing requisite moles of DOPC and cholesterol, and 10 mol% of POPC-d_{31}. The dry lipids were subsequently dissolved in 1:1 v:v methanol:cyclohexane to obtain homogeneous mixing. The mixture was then dried to a powder under vacuum overnight. Multilamellar lipid dispersions were subsequently prepared by hydrating dry lipid powders with 10 mM, pH ≈ 8 sodium phosphate buffer (prepared in deuterium-depleted H_2O, weight fraction of 50 %, pH ≈ 8). One end of the NMR tube was flame-sealed to prevent water loss, and multilamellar dispersions were taken through 5 freeze-thaw cycles (using liquid nitrogen and a low temperature heat gun), with intermittent vortex mixing and centrifugation to ensure sample homogeneity.

Preparation of Multilamellar Vesicles (MLVs) for Electron Spin Resonance (ESR) Measurements. Samples were prepared by mixing 2 μmol of DOPC and cholesterol with 10 nmol of a lipid spin probe (16-PC or 1-palmitoyl-2-stearoyl-(16-doxyl)-*sn*-glycero-3-phosphocholine

labeled at the 16th Carbon position) in chloroform. Cholesterol mol% was varied from 0 to 50 in steps of 10 mol%. The bulk solvent was removed with an argon stream for ≈ 15 min at 40 °C, followed by drying *in vacuo* overnight at room temperature. The dried films were hydrated with 400 μL of pre-warmed (40 °C) H_2O and incubated for 1 h at 40 °C, vortexing every 15 min. Samples were subjected to 5 freeze/thaw cycles using a –80 °C freezer and a water bath set to 40 °C. The resulting MLVs were centrifuged (13,000 rpm) at room temperature for 30 min. Roughly 350 μL of supernatant was then removed from each sample and the pellets were dissolved with the remaining 50 μL of H_2O.The concentrated samples were loaded into open-ended (1.5 to 1.8 mm) × 100 mm glass capillaries (Kimble Chase Life Science, Rockwood, TN). After flame sealing one end of the capillary, the sample was spun down with low speed centrifugation, and the other end was then flame sealed.

Methods

Small-Angle X-ray Scattering (SAXS). Vesicle samples for small-angle X-ray scattering (SAXS) measurements were prepared at 20 mg/mL, as described above. The SAXS data were collected at a fixed sample-to-detector distance (SDD) calibrated using a silver behenate standard, with a typical data collection time of 3 h. The one-dimensional scattering intensity $I(q)$ [$q = 4\pi \sin\theta/\lambda$, where λ is the X-ray wavelength and 2θ is the scattering angle relative to the incident beam] was obtained by radial averaging of the corrected 2D detector images, an operation that was performed using the Rigaku SAXSLab software. Data were collected in 10-min frames, with each frame processed separately to assess radiation damage; there were no significant changes observed in the scattering curves as a function of time. Background scattering was collected on the buffer using a flow-through capillary cell (Rigaku BioSAXS Automatic Sample Changer with fixed capillary cell). The background scattering was subtracted from each frame using proper scaling (see Fig. S1A). Background-corrected $I(q)$ from individual frames was then averaged with the standard deviation taken to be the measurement uncertainty and used in the weighted least-squares analyses.

Small-Angle Neutron Scattering (SANS). The SANS measurements were conducted on two sets of vesicle suspensions in D_2O buffer, either using tail-perdeuterated DOPC-d_{66} and Chol-d_{40} (Fig. 1B) or fully protiated DOPC-cholesterol mixtures (Fig. S1B). The former system provides enhanced contrast between the lipid head-groups, in addition to contrast between the bilayer and the buffer. The LUV suspensions were loaded into 1-mm path-length quartz banjo cells (Hellma USA, Plainview, NY) and mounted in a temperature-controlled cell holder with ≈ 1 °C accuracy. All measurements were performed at 25 °C. Measurements were performed on the NGB-30m SANS instrument at the NIST Center for Neutron Research (NCNR) using the standard SANS configuration (λ = 6.0 Å and SDDs of 1 m, 4 m, and 13 m) combined with the lens configuration (λ = 8.4 Å and SDD of 13 m), accessing an overall *q*-range between ≈ 0.001 $Å^{-1}$ and 0.5 $Å^{-1}$. The 2D scattering signals were normalized and corrected for resolution, empty cell scattering, and background using the NCNR Igor data reduction software (4). The same software was used to obtain the 1D SANS patterns (see Fig. 1B and S1B) by circularly averaging the normalized 2D data and subsequently stitching data sets over adjacent *q*-ranges accessed by the different instrument configurations stated above. Two sets of SANS measurements were performed on each sample with concentrations of 50 mg/mL and 20 mg/mL. The higher concentration samples matched those used in neutron spin-echo measurements, and the 20 mg/mL samples were obtained by diluting the more concentrated samples, and were measured for data fitting purposes – specifically to eliminate any possible structure factor contributions that could interfere with the fitting procedure (see scattering analysis section below).

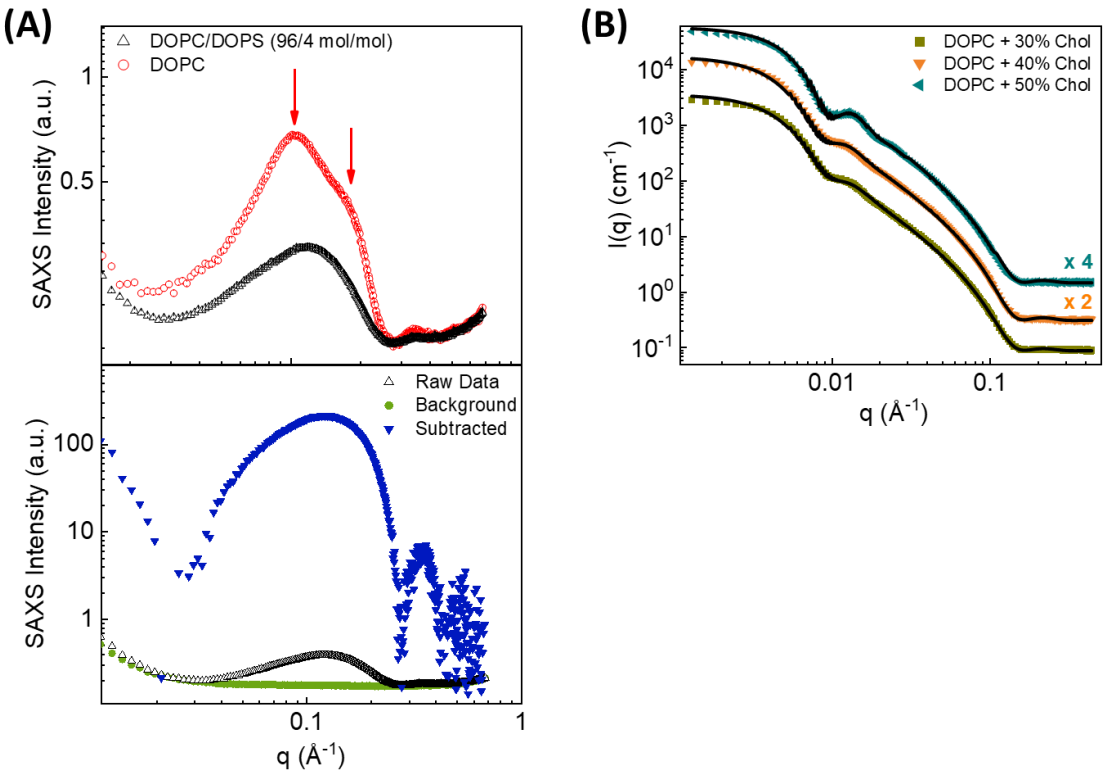

Fig. S1. (A) Top: Raw (uncorrected) SAXS data of extruded DOPC membranes with (black triangle) and without (red circles) the inclusion of anionic charged DOPS lipid. In the absence of DOPS, the signature of multilamellar vesicles is still observed even after multiple extrusions. (A) Bottom: Example of raw data for a DOPC/DOPS sample, background scattering from the buffer, as well as the background-subtracted data (rescaled ×1000) used in the SAXS analysis. (B) SANS data and corresponding fits (obtained with the SasView Software) of fully protiated DOPC-Chol vesicles containing (30, 40, and 50) mol% cholesterol in deuterated buffer. Measurements were performed at a sample concentration of 20 mg/mL. Data sets are shifted vertically for clarity. Error bars represent ±1 standard deviation in all figures, and may be smaller than the symbol size.

Small-Angle Scattering Analysis. Scattering data were analyzed following Doktorova *et al.* (5) with modifications described herein. The experimentally observed scattering intensity from a vesicle suspension can be expressed as the product of a single-bilayer vesicle form factor $P(q)$ and a structure factor $S(q)$ that accounts for density correlations between different bilayers, i.e.:

$$I(q) = q^{-2}P(q)S(q)\,. \qquad Eq.S1$$

For dilute unilamellar vesicles, such as those used here, $S(q) \approx 1$. Pencer *et al.* (6) showed that, for a polydisperse vesicle suspension whose sizes follow a Schulz distribution, $P(q)$ is well-approximated by

$$P(q) \approx P_{\mathrm{V}}(R_{\mathrm{m}}, \sigma, q)|F_{\mathrm{B}}(q)|^2\,, \qquad Eq.S2$$

where R_{m} is the average vesicle radius, σ is the relative size polydispersity, and $P_{\mathrm{V}}(R_{\mathrm{m}}, \sigma, q)$ accounts for the influence of vesicle size and shape on the scattering intensity, such that

$$P_{\mathrm{V}}(R_{\mathrm{m}},\sigma,q) = 8\pi^2 {R_{\mathrm{m}}}^2\sigma^4(1+\sigma^{-2})(2+\sigma^{-2}) \times\left[1-\frac{\left(1+4q^2{R_{\mathrm{m}}}^2\sigma^4\right)^{-\frac{1}{2\sigma^2}}\cos\left((2+\sigma^{-2})\tan^{-1}(2qR_{\mathrm{m}}\sigma^2)\right)}{1+4q^2{R_{\mathrm{m}}}^2\sigma^4}\right]. \qquad Eq.S3$$

The flat bilayer scattering amplitude $F_{\mathrm{B}}(q)$ in Eq. S2 accounts for density correlations within a single bilayer, normal to the plane of the bilayer (i.e., the lipid bilayer transverse structure). We model F_{B} using a symmetric six-slab volume probability distribution with separate components for the lipid headgroups, combined with the CH and CH_2 groups of the hydrocarbon chains and terminal CH_3 groups found at the bilayer midplane (5):

$$F_{\mathrm{B}}(q) = \frac{2e^{-\frac{(q\sigma_S)^2}{2}}}{qD_{\mathrm{H}}A_{\mathrm{L}}V_{\mathrm{T}}V_{\mathrm{W}}(V_{\mathrm{C}}-2V_{\mathrm{T}})}\Big|V_{\mathrm{T}}\{b_{\mathrm{W}}(A_{\mathrm{L}}D_{\mathrm{H}}-V_{\mathrm{H}})(V_{\mathrm{C}}-2V_{\mathrm{T}})+V_{\mathrm{W}}b_{\mathrm{H}}(V_{\mathrm{C}}-2V_{\mathrm{T}}) - V_{\mathrm{W}}A_{\mathrm{L}}D_{\mathrm{H}}(b_{\mathrm{C}}-2b_{\mathrm{T}})\}\sin\left(\frac{qV_{\mathrm{C}}}{A_{\mathrm{L}}}\right)+V_{\mathrm{T}}(V_{\mathrm{C}}-2V_{\mathrm{T}})(b_{\mathrm{W}}V_{\mathrm{H}}-b_{\mathrm{H}}V_{\mathrm{W}})\sin\left(qD_{\mathrm{H}}+\frac{qV_{\mathrm{C}}}{A_{\mathrm{L}}}\right) + V_{\mathrm{W}}A_{\mathrm{L}}D_{\mathrm{H}}(b_{\mathrm{C}}V_{\mathrm{T}}-b_{\mathrm{T}}V_{\mathrm{C}})\sin\left(\frac{2qV_{\mathrm{T}}}{A_{\mathrm{L}}}\right)\Big| . \qquad Eq.S4$$

In Eq. S4, V_{C}, V_{H}, V_{T}, and V_{W} are the molecular volumes of the lipid hydrocarbon chains, headgroup, terminal methyl, and water, respectively, with corresponding scattering factors b_{C}, b_{H}, b_{T}, and b_{W}. Each of these values was constrained in the analyses: V_{C} and V_{H} were obtained from the literature (Table S1), V_{T} and V_{W} were fixed at 55 Å^3 and 30.1 Å^3, respectively, and scattering factors were calculated from the atomic compositions. To mimic the smoothing effects of thermal disorder, the step-like volume probability profile was convoluted with a Gaussian of width σ_{S} = 2.5 Å. Of the remaining fit parameters, two are related to bilayer structure (i.e., the area per lipid, A_L, and the headgroup thickness, D_H) and two are related to the vesicle size distribution (R_{m} and σ). Additional bilayer structural parameters are derived from fitted model parameters, the most important of which are the total (Luzzati) bilayer thickness, $D_{\mathrm{B}} = 2(V_{\mathrm{C}}+V_{\mathrm{H}})/A_{\mathrm{L}}$, and the hydrocarbon thickness, $2D_{\mathrm{C}} = 2V_{\mathrm{C}}/A_{\mathrm{L}}$. Note that the electron density profiles obtained from the SAXS data fits yield the phosphate-to-phosphate (p-p) thickness reported in Table S2 and Fig. S2.

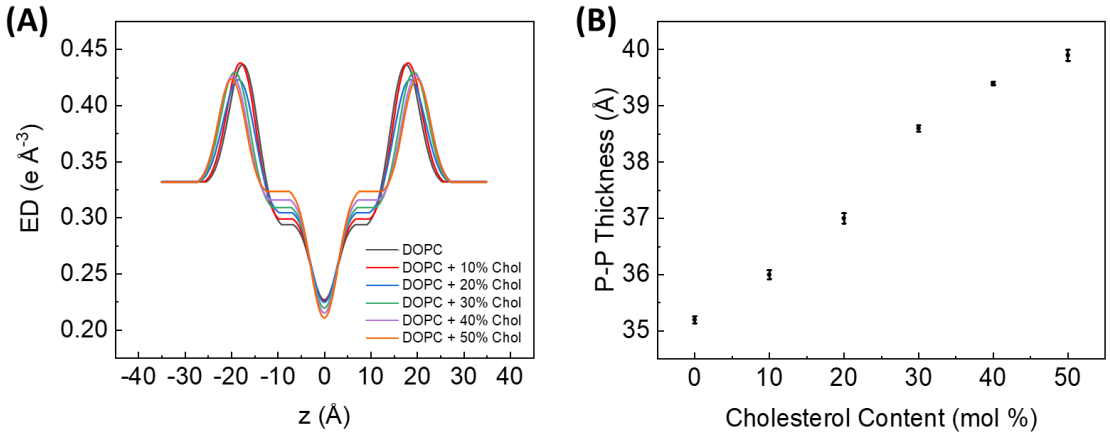

Fig. S2. (A) Electron density (ED) profiles along the membrane normal (*z*-axis) obtained from SAXS data for DOPC-Chol membranes, such that *z* = 0 denotes the center of the membrane. (B) Phosphate-to-phosphate thickness (p-p thickness) of DOPC-Chol membranes as a function of cholesterol content, measured as the peak-to-peak distance of the electron-rich phosphate groups in the ED profiles in panel (A). Error bars represent ±1 standard deviation as reported in Table S2.

Uncertainties in structural parameters were obtained from a Monte Carlo method (7). Briefly, a synthetic scattering data set consistent with experimental noise was generated as follows: $I_{\mathrm{syn}}(q) = I_{\mathrm{fit}}(q) + X(q)$, where $X(q) \sim \mathcal{N}\left[0, \sigma_{\mathrm{exp}}(q)\right]$. In these equations, I_{fit} is the best-fit intensity value and X, which represents noise, is a random variable drawn from a Gaussian distribution whose standard deviation, σ_{exp}, corresponds to the experimentally determined uncertainty. Synthetic data sets for X-ray and neutron data were jointly analyzed as previously described (8) to determine how the structural parameters $A_{\mathrm{L,syn}}$, $D_{\mathrm{B,syn}}$, $2D_{\mathrm{C,syn}}$, and $D_{\mathrm{H,syn}}$ were affected by the propagation of errors. This process was repeated 100 times to generate populations of synthetic structural parameters; the uncertainties reported in Table S2 are the standard deviations of these populations.

Complementary SANS data analysis was performed using the built-in core/multi-shell model in the SasView software (9) by employing a three-shell vesicle model (head-tail-head). The model assumes a Schulz distribution of the vesicle radius that is fitted over the low *q*-range of the data. This model, however, does not take into account gradients in the interfaces between the headgroup and hydrocarbon layers due to the Gaussian distribution of different lipid subgroups (as discussed above). Results of this analysis are presented in Table S2 and compared to the more refined approach used in the joint fitting of the SANS and SAXS data as described earlier in this section. Note that fits to SANS data were done using a uniform background fit parameter to account for the incoherent background scattering from the hydrogen moieties in the sample (4). Examples of high *q*-range fits to SANS data from tail-deuterated vesicles and full *q*-range fits to data from protiated vesicles in deuterated buffer are shown in Fig. 1B and S1B, respectively.

Solid-State ^{2}H NMR Spectroscopy (Equilibrium Lineshapes). Unlike in the case of lipids, where one or both the saturated acyl chains are deuterated (POPC-d_{31} and DMPC-d_{54}, respectively), application of solid-state ^{2}H NMR spectroscopy to membranes composed of lipids with di-monounsaturated acyl chains (e.g., DOPC) is non-trivial. The geometry of the CH=CH segment precludes interpretation of the quadrupolar splittings and subsequent structural analysis. However, order parameters obtained from ^{2}H NMR reflect membrane properties averaged over the entire system that are influenced by inter-molecular interactions. Thus, it is possible to investigate the average structure of protiated-DOPC membranes by introducing small quantities of saturated acyl chain-deuterated lipids (such as POPC-d_{31}) as a probe, ensuring that the structural and physical properties of the original system are minimally impacted. Thus, solid-state ^{2}H NMR measurements were performed on protiated DOPC-Chol membranes containing 10 mol% POPC-d_{31}. Powder type spectra (Pake-patterns) were obtained by Fourier transformation of quadrupolar echoes, starting at the echo top with a fast Fourier transform algorithm (10) using an in-house MATLAB routine. The solid-state ^{2}H NMR spectra were numerically inverted using the de-Pakeing method to obtain equilibrium spectrum (Fig. S3) corresponding to a θ = 0° bilayer orientation relative to the external magnetic field (11).

Segmental order parameters $S_{\mathrm{CD}}^{(i)}$ of C–^{2}H bonds (Fig. S4A) were obtained using:

$$\left|\Delta\nu_{\mathrm{Q}}^{(i)}\right| = \frac{3}{2}\chi_{\mathrm{Q}}\left|S_{\mathrm{CD}}^{(i)}\right|\left|P_2(\cos\theta)\right| \qquad Eq.S5$$

where $\Delta\nu_{\mathrm{Q}}^{(i)}$ is the *i*th residual quadrupolar splitting, χ_{Q} is the static quadrupolar coupling constant (170 kHz) and $P_2(\cos\theta) = \frac{1}{2}(3\cos^2(\theta) - 1)$. Here θ represents the orientation of the membrane normal (director) with respect to the main magnetic field ($\mathbf{B}_0$). $P_2(\cos\theta) = \frac{1}{2}(3\cos^2(\theta) - 1)$ and $S_{\mathrm{CD}}^{(i)} = P_2\left(\cos\beta^{(i)}\right) = \frac{1}{2}(3\cos^2\left(\beta^{(i)}\right) - 1)$ where $\beta^{(i)}$ is the orientation of the symmetry axis of internal frame of the CH_2 segment with respect to the director. The order profiles in Fig. S4A include a plateau and subsequently a reduction in orientational order of the acyl core region of the bilayer. Absolute order parameters for DOPC membranes in the plateau region are nearly two times smaller ($S_{\mathrm{CD}} \approx 0.2$) compared to order parameters in membranes with 50 mol% Chol ($S_{\mathrm{CD}} \approx 0.35$). Cholesterol addition leads to increased order parameters due to the reduction in area per lipid (Fig. 1, main text and Table S3) and an increase in hydrocarbon thickness, $2D_{\mathrm{C}}$ (Fig. S4B). The steric

thickness, D_B', (Fig. S4B) can be easily calculated from the bilayer hydrocarbon thickness, $2D_C$, by adding $2D_H$ (head group thicknesses) = 18 Å.

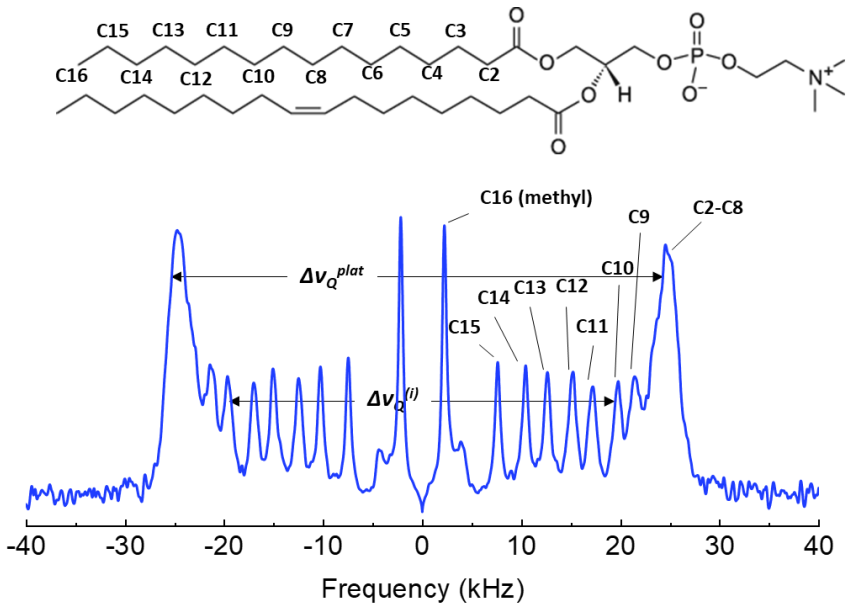

Fig. S3. Representative solid-state ^{2}H NMR de-Paked sub-spectrum (θ = 0°) of a multilamellar dispersion of pure DOPC (lamellar liquid crystalline L_α phase, 25 °C). Sample contains 10 mol% POPC-d_{31}.

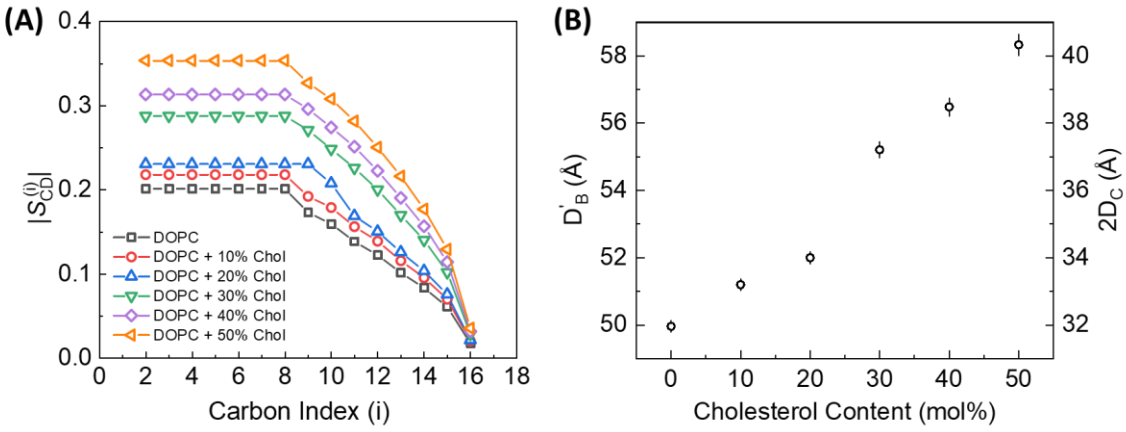

Fig. S4. (A) Segmental order parameter versus acyl position for POPC-d_{31} in DOPC-Chol membranes with different mol% cholesterol at T = 25 °C. Errors are on the order of 1% of the measured values and are smaller than the symbol size. (B) Structural parameters, i.e., steric thickness ($\boldsymbol{D_B'}$) and bilayer hydrocarbon thickness ($2D_C$), obtained from ^{2}H NMR lineshapes using the first-order mean-torque model.

Electron Spin Resonance (ESR) Analysis. ESR spectra were recorded on a Bruker EleXsys-II E500 CW ESR spectrometer operating at X-band frequency (9.4 GHz). The spectrometer settings for all samples were as follows: center field = 3362.9 × 10^{-4} T, sweep width = 10^{-2} T, microwave power = 0.3170 mW, modulation frequency = 100 kHz, modulation amplitude = 0.8 × 10^{-4} T, resolution (points) = 1024. Reported spectra are the average of 4 to 16 scans, depending on the signal intensity. Measurements were performed at 25 °C. To ensure proper temperature control, sealed capillaries containing the sample were placed into a 2-mm NMR tube containing light mineral oil. The ESR first derivative spectra were integrated once to obtain the corresponding absorbance spectrum, and then a second time, to obtain the total area, which is proportional to the total amount of spin probe in the sample; the areas were used as normalization factors for the first derivative spectra to correct for sample-to-sample differences in concentration. Normalized spectra were then re-centered to align the second absorbance peak at 3320 G. The normalized and centered ESR spectra of lipid samples with varying cholesterol content are shown in Fig. S5A. The uncorrected (apparent) order parameter S_{app} is given by (12, 13):

$$S_{\mathrm{app}} = \frac{A_{\mathrm{max}} - A_{\mathrm{min}}}{A_{zz} - 0.5(A_{xx} + A_{yy})}, \qquad Eq.S6$$

The principal components of the hyperfine tensor A_{xx}, A_{yy}, and A_{zz} used in our calculations, namely $(A_{xx}, A_{yy}, A_{zz}) = (5.0, 5.0, 32.6) \times 10^{-4}$ T were previously reported in the literature (14) for 16-PC in a similar lipid environment. The order parameters obtained from ESR measurements on DOPC-Chol membranes are shown in Fig. S5B as a function of increasing cholesterol content. The results are in excellent agreement with the order parameters obtained from RSF-MD simulations (described later).

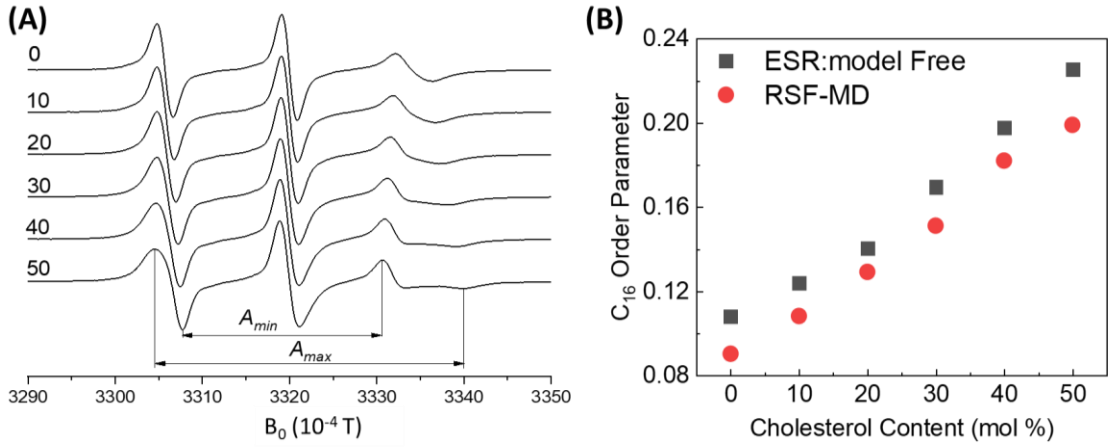

Fig. S5. (A) The first derivative ESR spectra of DOPC-Chol membranes with varying cholesterol content (mol%). The empirical parameters A_{min} and A_{max} (indicated by the arrowed lines) were used for calculations of the apparent order parameter, S_{app}. (B) Order parameter of DOPC-Chol membranes as measured by ESR and by RSF-MD simulations at the 16$^{\mathrm{th}}$ Carbon position along the acyl chain. The results show a significant increase in chain ordering with increasing cholesterol content, in agreement with SAXS/SANS results.

Neutron Spin Echo (NSE) Spectroscopy. NSE measurements were performed on 50 mg/mL suspensions of 50-nm and 100-nm diameter vesicles of DOPC:DOPS:Chol, in protiated and tail-perdeuterated forms, prepared in deuterated buffer, as discussed in the Materials and Methods section. Protiated and tail-deuterated samples were loaded in quartz cells with a path length of 2 mm and 4 mm, respectively, for optimal scattering signal. The NSE experiments on the NG-A NSE spectrometer at NCNR were conducted over a *q*-range of 0.04 $Å^{-1}$ to 0.1 $Å^{-1}$ for protiated vesicles and 0.04 $Å^{-1}$ to 0.18 $Å^{-1}$ for tail-perdeuterated vesicles. Analogous measurements were run on the deuterated buffer and on carbon black (sample for instrumental resolution) for background subtraction and data normalization, performed using the Data Analysis and Visualization Environment (DAVE) software developed at NIST (15). Additional experiments on DOPC membranes with 20 mol% Chol were performed at the SNS-NSE spectrometer over a *q*-range of 0.05 $Å^{-1}$ to 0.15 $Å^{-1}$. The instrument resolution and the D_2O buffer were measured under the same configurations for data reduction and normalization. The data reduction was done using the ECHODET software of SNS-NSE spectrometer, which generates the $I(q,t)/I(q,0)$ data sets required for the characterization of membrane dynamics. Subsequent data fitting and analysis were performed using Python scripts developed in house, following the same protocols described below for the NCNR-NSE data. Data sets obtained from identical samples on the two spectrometers yielded the same fit results, within the margin of error.

NSE Analysis. The reduced NSE data yield the normalized intermediate scattering function $I(q,t)/I(q,0)$ for discrete *q*-values within the accessed *q*-range, where *t* is the Fourier time. For lipid membranes, the probed dynamics follow a stretched exponential function with a stretching exponent of 2/3, such that (16):

$$I(q,t)/I(q,0) = \exp\left[-(\Gamma(q)t)^{2/3}\right], \quad Eq.S8$$

Fits of the intermediate scattering functions using Eq. S8 yield the decay rate, $\Gamma(q)$, at individual *q*-values (see Fig. 2A and Fig. S6). Fits of Γ(*q*) vs. *q* for protiated vesicles yielded the effective bending rigidity modulus of DOPC-Chol membranes for cholesterol content from 0 mol% to 50 mol%, as indicated in Eq. 1. For tail-deuterated vesicles formed of DOPC-d_{66} and Chol-d_{40}, the decay rates showed an enhancement on top of bending dynamics and were fitted to Eq. 2. In Eq. 2, the area compressibility modulus, K_A, was calculated from the bending rigidity modulus, κ, as measured from bending fluctuation signals on analogous protiated vesicles. Calculations of K_A were done according to the polymer brush model, i.e., $K_A = 24\kappa/(2D_c)^2$, for DOPC membranes. For cholesterol-containing membranes, we followed the modified polymer brush model introduced by Doktorova et al. (17). In their model, and to account for the incompressible regions around the sterol ring, they substituted the mechanical thickness $2D_C$ by (p-p thickness – 2 × 7 Å) for membranes containing 10 mol% cholesterol, and by (p-p thickness – 2 × 8 Å) for membranes containing more than 20 mol% cholesterol. Here, we follow the same formalism. However, comparisons of the simulation and experimental p-p thickness showed a difference of 4 Å. We thus adjusted for this difference in our K_A calculations (see Table S5). We note that the obtained K_A values are in excellent agreement with previous experimental results by Evans *et al*. (18) and with the simulation results of Doktorova *et al.* (17). We also note that the thickness fluctuation fits were performed by taking into account the instrumental *q*-resolution (treated as a convolution of Eq. 2 with a Gaussian distribution of a fixed width), following the approach of Nagao *et al*. (19).

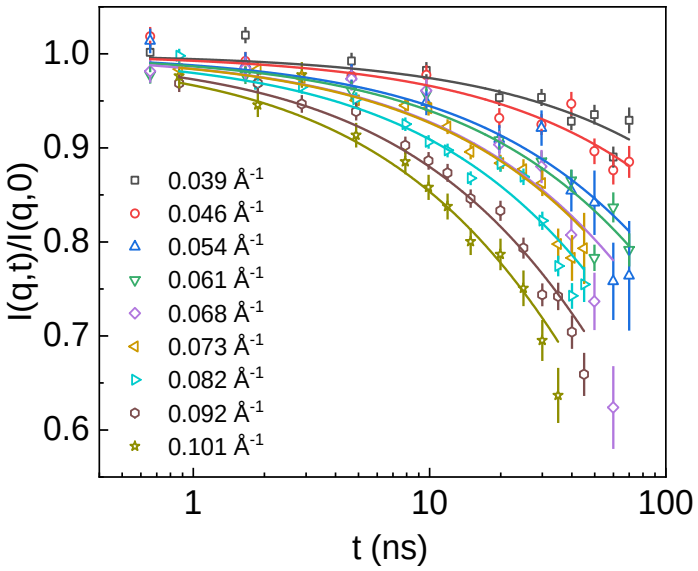

Fig. S6. NSE-measured intermediate scattering functions on 50-nm vesicles of protiated DOPC membranes with 20 mol% Chol. Error bars represent ±1 standard deviation. The lines are fits to the data using a stretched exponential function (Eq. S8).

Solid-state ^{2}H NMR Spectroscopy (Spin-lattice relaxation experiment). Experimental ^{2}H NMR spectra were acquired with a Bruker AMX-500 spectrometer (11.78 T magnetic field strength, ^{2}H frequency 76.77 MHz). Powder-type spectra for the multilamellar lipid dispersions were recorded with a phase-cycled, quadrupolar echo sequence [i.e., $(\pi/2)_x - d_6 - (\pi/2)_y - d_7 -$ acquire]. A home-built solid-state probe with an 8-mm diameter coil and high-voltage capacitors (Polyflon, Norwal, CT) was used with a Bruker radiofrequency amplifier (B-SV 10 500 MHz) to generate 5-μs 90° pulses. The transient NMR signals were shunted to a preamplifier (Miteq; Hauppauge, NY) using a Lowe-Tarr series crossed-diode circuit and recorded using a Bruker fast digitizer. Typical spectral acquisition parameters involved a pulse spacing (d_6) of 40 μs, a dwell time of 0.5 μs, (d_7) of 20 μs and the collection of 16384 data points. Recycle times were generally 1 s and typically, 4096 transients were collected. Free induction decays were Fourier transformed beginning at the maximum of the quadrupolar (solid) echo. The radiofrequency coil was enclosed in a glass Dewar and the temperature was controlled with a flow of compressed air using a Bruker variable temperature controller (B-VT-2000) interfaced to a heater/sensor located in the probe. The temperature was monitored before and after each measurement with a thermistor inserted directly above the radiofrequency coil, and typically was found to vary by less than 1 °C during a given run. The samples were kept at the desired temperature for more than 30 min for temperature stabilization before experimentation. Temperatures were estimated to be accurate within ±1 °C of the reported values. The spin-lattice (Zeeman) relaxation times (T_{1Z}) were measured using an inversion recovery pulse sequence, i.e., $(\pi)_x - t - (\pi/2)_x - d_6 - (\pi/2)_y - d_7 -$ acquire. Spectra were recorded at 14 variable delays (t). Fig. S7A depicts inversion-recovery ^{2}H NMR spectra for a random multilamellar dispersion of DOPC in the L_α phase. After the inverting π pulse, z-magnetizations were negative and recovered to their equilibrium positive signal. The spin-lattice relaxation rates for each resolved peak were obtained by non-linear regression fitting (Fig. S7B) using the function $M(t) = M_0[1 - W\exp(-R_{1Z}t)]$, where $R_{1Z} = 1/T_{1Z}$ is the relaxation rate, M_0 is the signal intensity at equilibrium, and the incompleteness of the magnetic inversion is accounted for

by the parameter *W*. Subsequently, a square law functional dependence of $R_{1Z}^{(i)}$ on $S_{CD}^{(i)}$ can be observed in Fig. 3B (main text).

For the error analysis of the solid-state ^{2}H NMR relaxation times, the inversion-recovery spectra obtained with a quadrupolar echo pulse sequence (20) were numerically deconvoluted (de-Paked). The amplitudes were fit to a standard three-parameter relaxation function for the inversion recovery (i.e., an individual spectral peak) at the time delay *t* between the *π* inversion pulse and the quadrupolar-echo pulse sequence used to read out the longitudinal magnetization, where the spin-lattice (Zeeman) relaxation time T_{1Z} is the quantity to be determined. Estimated errors in the T_{1Z} relaxation times corresponded to the standard deviation as determined from nonlinear regression fitting (21), and assumed random statistical fluctuations in the data; systematic errors were not considered. In addition, the analysis does not consider cross-correlations among the fitting parameters. Analytical formulas for the calculated properties (22) were used, together with prorogation of errors to obtain the corresponding errors in the derived structural parameters.

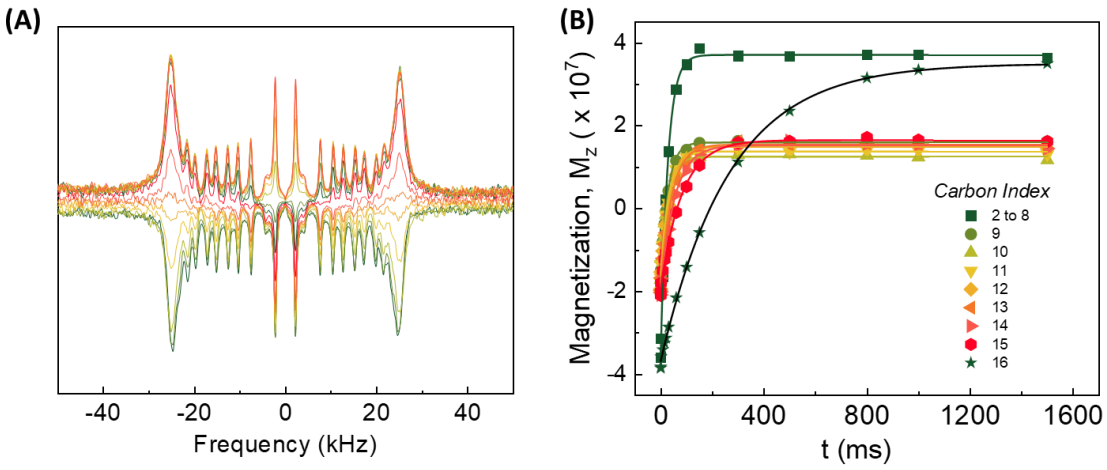

Fig. S7. (A) Typical inversion recovery spectra of ^{2}H nuclear magnetization for DOPC multilamellar dispersion (*T* = 25 °C) prepared in sodium phosphate buffer (pH ≈ 8, mass fraction of 50% deuterium depleted H_2O). (B) Spin-lattice relaxation rates for each peak were fitted to obtain the R_{1Z} relaxation rate. Data were acquired at 76.8 MHz using a phase-cycled, inversion-recovery quadrupolar echo pulse sequence with delays ranging from 0.01 ms (bottom) to 1.5 s (top). Error bars are on the order of 1×10^6 as calculated from baseline noise and are smaller than symbol size.

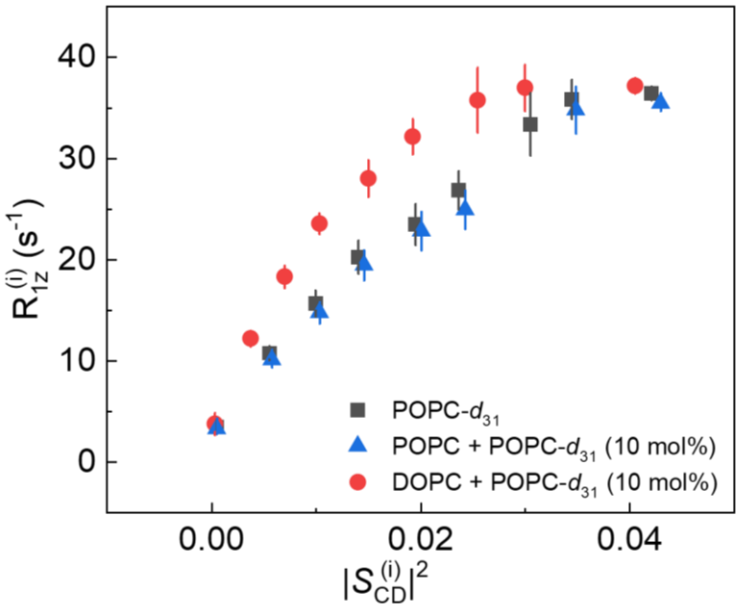

Fig. S8. The relaxation rates, R_{1Z}, measured using 10 mol% of the POPC-d_{31} probe in protiated POPC membranes match those measured in POPC-d_{31} membranes. The relative square-law slopes, as discussed in the main manuscript, indicate that DOPC membranes are "softer" than POPC membranes, as expected.

RSF-MD Simulation Protocol. Simulations were all-atom and constructed using the CHARMM-GUI server (23). Each bilayer contained a total of 200 lipids (100 lipids per leaflet) and was hydrated with 45 water molecules per lipid. Simulations were performed with the NAMD software (24) using the CHARMM36 force-field for lipids (25, 26) and systems were initially equilibrated following the CHARMM-GUI protocols. Subsequent production runs employed a 2-fs timestep with *rigidBonds* set to *all*. The potential for van der Waals interactions was switched at 10 Å and truncated at 12 Å using the CHARMM force switching function through the NAMD *vdwForceSwitching* option. Long-range electrostatic interactions were calculated using the Particle Mesh Ewald (PME) method with a 1 Å grid spacing. A constant temperature of 25 ºC (for the DOPC/Chol bilayers) or 37 ºC (for stearoylsphingomyelin (SSM) with 30% Chol) and a pressure of 1 atm were maintained with a Langevin thermostat (with a damping coefficient of 5 ps^{-1}) and barostat (with a piston period of 200 fs and piston decay of 50 fs), respectively. The total simulation time of the trajectories, as well as the corresponding lengths of the last parts used for analysis (as determined by convergence of lipid packing using the method by Chodera (27) for the DOPC/Chol systems are indicated in Table S5. The SSM/Chol bilayer was simulated for a total of 1050 ns and the last 600 ns were used for analysis.

RSF-MD Simulation Analysis. The bending rigidity was calculated from real-space analysis of local fluctuations of lipid splay angles, as described in a recent study by Doktorova *et al*. (28) and summarized in Table S5. Simulated DOPC-Chol bilayers were assembled by randomly placing equal numbers of cholesterol molecules in the two bilayer leaflets, and simulated until their bilayer areas converged. A director vector was defined for each DOPC and cholesterol molecule. The distribution of splay angles (i.e., angles between the molecular director vectors) was calculated for each unique pair of lipids, i.e., DOPC-DOPC, Chol-Chol and DOPC-Chol, from the simulation trajectories by considering only neighboring lipids (i.e., lipids within 10 Å of one another). The resulting distributions were used to obtain a potential of mean force (PMF), from which the respective splay modulus of each lipid pair emerged from a quadratic fit to the PMF in the regime of small splay angles. The analysis was performed separately on each bilayer leaflet, and a

weighted average of the three splay moduli, corresponding to the three unique lipid pairs in the leaflet, produced the monolayer bending rigidity. The value of κ for the bilayer was then obtained from the sum of the two leaflets' bending moduli. The average area per lipid, A_{L}, was calculated by dividing the mean lateral area of the simulation box by 100 (the total number of lipids in a leaflet). The partial area of Chol, A_{Chol}, was approximated from the Cholesterol tilt angle following Eq. 8 in reference (29). The partial area of DOPC, A_{DOPC}, was then obtained from the mole fractions of DOPC and cholesterol, χ_{DOPC} and χ_{Chol} respectively, using the relationship (29):

$$A_{\mathrm{L}} = \chi_{\mathrm{DOPC}} A_{\mathrm{DOPC}} + \chi_{\mathrm{Chol}} A_{\mathrm{Chol}}, \quad Eq.S9$$

The orientational order parameter σ was obtained by calculating the splay angle β and the lateral (2D) distance d between every pair of DOPC (or SSM) lipids in each leaflet and using (30):

$$\sigma = \frac{1}{2}\langle 3\cos^2\beta - 1\rangle. \quad Eq.S10$$

The σ values were then binned according to the corresponding distances between the lipids (calculated using the center of mass of the lipids) and the average σ in each bin was plotted as a function of d (Fig. S9A).

The splay autocorrelation time τ for each bilayer was calculated from the time evolution of the splay angle between each pair of DOPC (or SSM) lipids using the MATLAB *acf* function with standard rejection value assuming white noise. The τ values for all lipid pairs in each leaflet of the bilayers were then used to construct histograms of probability distributions as shown in Fig. S9B.

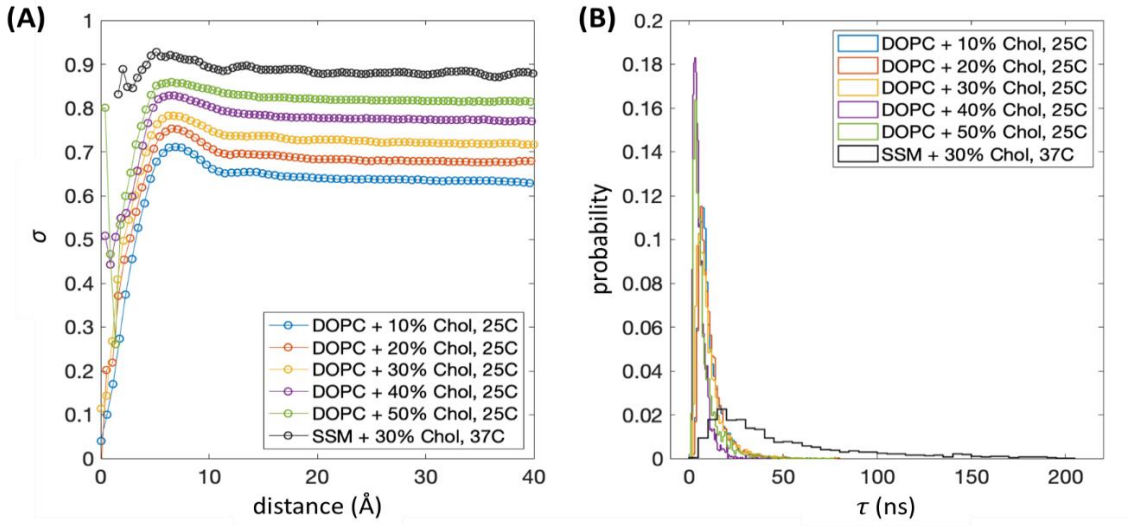

Fig. S9. (A) Orientational order parameter, σ, averaged over all lipid pairs as a function of positional separation. Order parameters were calculated in MD simulations for DOPC-Chol bilayers as well as, sphingomyelin (SSM) bilayers with 30% Chol. (B) Probability distributions of the autocorrelation times of the splay angles shows that they extend beyond 100 ns in the SSM-Chol simulation, whereas all DOPC-Chol bilayers are characterized by autocorrelation times shorter than ≈ 25 ns.

Disclaimer. Certain trade names and company products are identified in order to specify adequately the experimental procedure. In no case does such identification imply recommendation or endorsement by the National Institute of Standards and Technology, nor does it imply that the products are necessarily the best for the purpose.

Table S1. Volumes and scattering factors of lipids used in the fits of small-angle scattering data: $\boldsymbol{V_L}$, total lipid volume; $\boldsymbol{V_H}$, headgroup volume; $\boldsymbol{V_C}$, hydrocarbon volume; $\boldsymbol{b_H^X}$, headgroup X-ray scattering factor; $\boldsymbol{b_H^N}$, headgroup neutron scattering factor; $\boldsymbol{b_C^X}$, hydrocarbon X-ray scattering factor; $\boldsymbol{b_C^N}$, hydrocarbon neutron scattering factor. X-ray scattering factors are calculated as the total number of electrons of the constituent atoms (neglecting the *q*-dependence), and neutron scattering factors are calculated as the sum of atomic neutron scattering lengths of the constituent atoms.

Lipid	V_C [Å^3]	V_H [Å^3]	b_H^X [e$^-$]	b_H^N [fm Å^{-3}]	V_C [Å^3]	b_C^X [e$^-$]	b_C^N [fm Å^{-3}]
DOPC[a]	1298	331	164	60.072	967	270	-20.81
DOPC-d_{66}[b]	1298	331	164	60.072	967	270	666.25
Chol[c]	629	18	9	12.474	611	207	11.187
Chol-d_{40}[d]	629	18	9	12.474	611	207	427.587

[a] Kučerka et al. (31); [b] volume assumed identical to DOPC; [c] Greenwood et al. (32); [d] volume assumed identical to Chol.

Table S2. Membrane structural parameters obtained from the fits to the SANS and SAXS data as described in the small-angle scattering analysis section above. Parameters reported here include the phosphate-to-phosphate (p-p) thickness, hydrocarbon chain thickness ($2D_C$), total bilayer thickness (D_B), and average area per lipid (A_L).

% Chol	*p-p thickness* [Å] (SAXS)	$2D_C$ [Å] joint	D_B [Å] joint	D_B [Å] 3-shell model	A_L [Å^2] joint	A_L [Å^2] 3-shell model
0	35.20 ± 0.06	28.6 ± 0.2	38.4 ± 0.3	38.3 ± 0.1	67.6 ± 0.4	67.6 ± 0.2
10	36.00 ± 0.08	29.6 ± 0.3	39.1 ± 0.4	40.1 ± 0.2	63.0 ± 0.6	61.3 ± 0.2
20	37.00 ± 0.08	29.7 ± 0.4	38.5 ± 0.5	41.2 ± 0.3	60.3 ± 0.8	56.5 ± 0.3
30	38.60 ± 0.01	32.3 ± 0.1	41.1 ± 0.1	43.3 ± 0.4	53.5 ± 0.1	50.7 ± 0.5
40	39.40 ± 0.03	33.4 ± 0.2	41.6 ± 0.1	43.8 ± 0.4	49.6 ± 0.1	47.2 ± 0.4
50	39.90 ± 0.09	34.9 ± 0.3	42.4 ± 0.1	44.3 ± 0.5	45.4 ± 0.1	43.7 ± 0.5

Table S3. Structural parameters, i.e., steric thickness (D'_B) and average area per lipid (A_L), obtained from solid-state ^{2}H NMR analysis using the mean torque model.

% Chol	D'_B [Å]	A_L [Å^2]
0	49.96 ± 0.17	61.53 ± 0.30
10	51.20 ± 0.17	59.23 ± 0.31
20	52.00 ± 0.18	57.84 ± 0.31
30	55.21 ± 0.24	52.85 ± 0.35
40	56.48 ± 0.27	51.11 ± 0.36
50	58.33 ± 0.31	48.76 ± 0.39

Table S4. Membrane parameters obtained from NSE data analysis, as described in the main text. *K_A is calculated according to the polymer brush model and K_A according to the modified polymer brush model as described above. Errors represent ±1 standard deviation.

% Chol	κ [k_BT] (50 nm LUVs)	κ [k_BT] (100 nm LUVs)	*K_A [mN/m] (100 nm LUVs)	K_A [mN/m] (100 nm LUVs)	μ [nPa.s.m]
0	13.01 ± 0.37	19.05 ± 0.65	230 ± 8	230 ± 8	16.72 ± 1.09
10	-	22.46 ± 1.77	253 ± 20	325 ± 26	26.31 ± 2.16
20	18.09 ± 0.64	30.34 ± 2.47	339 ± 28	471 ± 38	31.92 ± 3.49
30	23.15 ± 0.58				
40	30.31 ± 1.04				
50	38.81 ± 1.63				

Table S5. Structural and mechanical membrane parameters obtained from MD simulations for DOPC/Chol mixtures. Shown also are the full trajectory lengths and the corresponding parts used for analysis.

% Chol	Simulation time [ns]		A_L [Å²]	κ [k_BT]			order parameter C16, *sn*-2	p-p thickness
	total	used		top	bottom	bilayer		
0	523	517	68.2 ± 0.09	9.5 ± 0.3	8.8 ± 0.1	18.3 ± 0.3	0.090 ± 0.000	38.5 ± 0.04
10	336	336	62.3 ± 0.11	10.6 ± 0.2	11.9 ± 0.3	22.5 ± 0.4	0.108 ± 0.001	39.9 ± 0.06
20	350	350	56.9 ± 0.07	14.7 ± 0.3	15.8 ± 0.5	30.5 ± 0.6	0.129 ± 0.001	41.5 ± 0.04
30	631	355	52.0 ± 0.09	19.1 ± 0.5	18.9 ± 0.4	38.0 ± 0.6	0.151 ± 0.001	43.0 ± 0.06
40	781	178	47.6 ± 0.06	25.9 ± 0.5	26.2 ± 0.6	52.1 ± 0.8	0.182 ± 0.001	44.4 ± 0.05
50	792	360	44.2 ± 0.07	34.7 ± 0.8	33.0 ± 0.7	67.7 ± 1.1	0.199 ± 0.001	45.1 ± 0.04

SI References

1. Mena PL & Djerassi C (1985) Synthesis of 5,9-hexacosadienoic acid phospholipids. 11. Phospholipid studies of marine organisms. *Chem. Phys. Lipids* 37(3):257-270.
2. Nickels JD*, et al.* (2015) Mechanical Properties of Nanoscopic Lipid Domains. *J. Am. Chem. Soc.* 137(50):15772-15780.
3. Scott HL*, et al.* (2019) On the Mechanism of Bilayer Separation by Extrusion, or Why Your LUVs Are Not Really Unilamellar. *Biophys. J.* 117(8):1381-1386.
4. Kline S (2006) Reduction and analysis of SANS and USANS data using IGOR Pro. *J. Appl. Cryst.* 39(6):895-900.
5. Doktorova M*, et al.* (2019) Gramicidin Increases Lipid Flip-Flop in Symmetric and Asymmetric Lipid Vesicles. *Biophys. J.* 116(5):860-873.
6. Pencer J, Krueger S, Adams CP, & Katsaras J (2006) Method of separated form factors for polydisperse vesicles. *J. Appl. Cryst.* 39(3):293-303.
7. Press WH, Flannery BP, Teukolsky SA, & Vetterling WT (1992) *Numerical Recipes in C: The Art of Scientific Computing* (Cambridge University Press) 2nd edition Ed.
8. Kučerka N, Pencer J, Nieh MP, & Katsaras J (2007) Influence of cholesterol on the bilayer properties of monounsaturated phosphatidylcholine unilamellar vesicles. *Eur. Phys. J. E* 23(3):247-254.
9. http://www.sasview.org/.
10. McCabe MA & Wassail SR (1997) Rapid deconvolution of NMR powder spectra by weighted fast Fourier transformation. *Solid State Nucl. Magn. Reson.* 10(1):53-61.
11. Sternin E, Schäfer H, Polozov IV, & Gawrisch K (2001) Simultaneous Determination of Orientational and Order Parameter Distributions from NMR Spectra of Partially Oriented Model Membranes. *J. Magn. Reson.* 149(1):110-113.
12. McConnell HM & Hubbell WL (1971) Molecular motion in spin-labeled phospholipids and membranes. *J. Am. Chem. Soc.* 93(2):314-326.
13. Gaffney BJ (1976) Practical considerations for the calculation of order parameters for fatty acid or phospholipid spin labels in membranes. *Spin Labelling. Theory and Applications*.
14. Smith AK & Freed JH (2012) Dynamics and ordering of lipid spin-labels along the coexistence curve of two membrane phases: An ESR study. *Chem. Phys. Lipids* 165(3):348-361.
15. Azuah RT*, et al.* (2009) DAVE: a comprehensive software suite for the reduction, visualization, and analysis of low energy neutron spectroscopic data. *J. Res. Natl. Inst. Stand. Technol.* 114(6):341-358.
16. Zilman AG & Granek R (1996) Undulations and Dynamic Structure Factor of Membranes. *Phys. Rev. Lett.* 77(23):4788-4791.
17. Doktorova M, LeVine MV, Khelashvili G, & Weinstein H (2019) A New Computational Method for Membrane Compressibility: Bilayer Mechanical Thickness Revisited. *Biophys. J.* 116(3):487-502.
18. Evans E, Rawicz W, & Smith BA (2013) Concluding remarks Back to the future: mechanics and thermodynamics of lipid biomembranes. *Faraday Discuss.*161(0):591-611.
19. Nagao M, Kelley EG, Ashkar R, Bradbury R, & Butler PD (2017) Probing Elastic and Viscous Properties of Phospholipid Bilayers Using Neutron Spin Echo Spectroscopy. *J. Phys. Chem. Lett.* 8(19):4679-4684.
20. Trouard TP, Alam TM, & Brown MF (1994) Angular dependence of deuterium spin-lattice relaxation rates of macroscopically oriented dilauroylphosphatidylcholine in the liquid-crystalline state. *J. Chem. Phys.* 101(6):5229-5261.
21. Bevington DK & Robinson PR (1992) *Data Reduction and Error Analysis for the Physical Sciences* (McGraw-Hill) 2nd edition Ed.
22. Petrache HI, Dodd SW, & Brown MF (2000) Area per Lipid and Acyl Length Distributions in Fluid Phosphatidylcholines Determined by 2H NMR Spectroscopy. *Biophys. J.* 79(6):3172-3192.
23. Jo S, Kim T, Iyer VG, & Im W (2008) CHARMM-GUI: A web-based graphical user interface for CHARMM. *J. Comput. Chem.* 29(11):1859-1865.
24. Phillips JC*, et al.* (2005) Scalable molecular dynamics with NAMD. *J. Comput. Chem.* 26(16):1781-1802.

25. Klauda JB*, et al.* (2010) Update of the CHARMM All-Atom Additive Force Field for Lipids: Validation on Six Lipid Types. *J. Phys. Chem. B* 114(23):7830-7843.
26. Pastor RW & MacKerell AD (2011) Development of the CHARMM Force Field for Lipids. *J. Phys. Chem. Lett.* 2(13):1526-1532.
27. Chodera JD (2016) A Simple Method for Automated Equilibration Detection in Molecular Simulations. *J. Chem. Theory Comput.* 12(4):1799-1805.
28. Doktorova M, Harries D, & Khelashvili G (2017) Determination of bending rigidity and tilt modulus of lipid membranes from real-space fluctuation analysis of molecular dynamics simulations. *Phys. Chem. Chem. Phys.* 19(25):16806-16818.
29. Alwarawrah M, Dai J, & Huang J (2010) A Molecular View of the Cholesterol Condensing Effect in DOPC Lipid Bilayers. *J. Phys. Chem. B* 114(22):7516-7523.
30. Khelashvili G, Pabst G, & Harries D (2010) Cholesterol Orientation and Tilt Modulus in DMPC Bilayers. *J. Phys. Chem. B* 114(22):7524-7534.
31. Kučerka N*, et al.* (2009) Areas of Monounsaturated Diacylphosphatidylcholines. *Biophys. J.* 97(7):1926-1932.
32. Greenwood AI, Tristram-Nagle S, & Nagle JF (2006) Partial molecular volumes of lipids and cholesterol. *Chem. Phys. Lipids* 143(1):1-10.